Supplementary Appendix

Clinical definitions

Diagnosis of cardiac amyloidosis

Based on the non-invasive diagnostic algorithm by Gillmore and colleagues in June 2016 (1), ATTR-CA was diagnosed in patients with significant myocardial tracer uptake (Perugini grade ≥2) on bone scintigraphy and absence of paraprotein detected by serum immunofixation, urine immunofixation, and serum assay for free light chains. After 2016, the collection of endomyocardial biopsies for the diagnosis of ATTR became necessary only when non-invasive test results were ambiguous or unclear. If cardiac ATTR was diagnosed, patients were offered sequencing of the TTR gene. Cardiac light-chain amyloidosis (AL) was diagnosed, if myocardial or extra-myocardial biopsy samples stained positive for Congo red, showed apple green birefringence under polarized light and reacted with light-chain antibodies during immunohistochemical staining. When extra-myocardial biopsy revealed the presence of amyloid fibrils, cardiac involvement was confirmed according to current recommendations (2).

Detailed information on electrocardiographic imaging

All maps (voltage, activation, potential) were projected onto normalised and co-registered anatomical heart surface models of the right and left ventricles. In order to map anatomical regions across patients, we have co-registered all models to one reference model. Of all anatomical models, the reference model with the best alignment for all patients was selected. The alignment was rated by evaluating the Euclidean distance between the models. Registration of anatomical models was performed in a multi-step approach: For initial alignment, we minimised the distance of the centroids between the models by translation, followed by an affine transformation using an iterative closest point algorithm (3). The final alignment was achieved by a non-rigid registration using an iterative closest point algorithm (4). All spatial models were normalized by down-sampling to the same number of vertices. An experienced cardiologist manually segmented the surface of the cardiac reference model according to 19

Schrutka L, *et al. Heart* 2022; 108:1137–1147. doi: 10.1136/heartjnl-2021-319846

standardised anatomical areas (5).

Detailed information on ECG processing

12-lead surface ECG recordings from the day of ECGI mapping were available from all CA patients. The ECGs were recorded with standard clinical ECG devices (GE Healthcare, Chicago, Illinois, USA) and printed on thermal paper with a feed rate of 25 mm/sec at 600 Hz sampling rate. ECGs were later scanned with a standard flatbed scanner (HP Development Company LP, Dallas, Texas, USA) at 600 dpi and ECG traces were separated from the background using a color threshold. Individual ECG trace values were iteratively reconstructed from pixel traces and low pass filtered for compensating aliasing effects. In case of missing pixels, the ECG trace was linearly interpolated. Three consecutive QRS complexes were manually annotated and extracted from the reconstructed ECG traces. The beginning of each QRS complex was normalised to the isoelectric line at 0mV. All QRS complexes were aligned by maximizing the cross-correlation.

Schrutka L, *et al. Heart* 2022; 108:1137–1147. doi: 10.1136/heartjnl-2021-319846

Supplementary Tables

Table S1. Baseline clinical and ECG characteristics of 221 ATTR and AL cardiac amyloidosis patients

	ATTR n=163	AL n=58	P value
Age, years (IQR)	77 (70-81)	73 (63-78)	**0.003**
Male gender, n (%)	128 (79.1)	36 (62.5)	**0.006**
Body mass index, kg/m^2 (IQR)	26 (24-28)	25 (23-29)	0.677
NYHA functional class ≥ II, n (%)	137 (84.2)	35 (59.7)	**<0.001**
NT-proBNP, pg/mL (IQR)	2387 (1134-3973)	3849 (1981-8472)	**0.004**
Mean pulmonary arterial pressure, mmHg (IQR)	30 (26-34)	33 (25-42)	0.328
Right atrial pressure, mmHg (IQR)	11 (7-15)	12 (7-18)	0.426
Pulmonary artery wedge pressure, mmHg (IQR)	19 (17-23)	22 (17-30)	0.145
Left ventricular end diastolic pressure, mmHg (IQR)	20 (16-25)	21 (19-26)	0.275
Left ventricular end-diastolic volume index, mL/m2 (IQR)	85.00 (74.00-96.34)	71.00 (58.24-79.41)	**<0.001**
Right ventricular end-diastolic volume index, mL/m2 (IQR)	88.57 (76.35-103.73)	74.93 (64.74-93.55)	**<0.001**
Interventricular septum, mm (IQR)	19 (17-22)	15 (13-18)	**0.010**
Left ventricular ejection fraction, % (IQR)	52 (43-59)	62 (56-65)	**<0.001**
Right ventricular ejection fraction, % (IQR)	47 (38-55)	55 (44-62)	**<0.001**
MOLLI-ECV, % (IQR)	48 (38-57)	43 (36-53)	0.177
Pleural effusion, n (%)	54 (33.1)	26 (44.1)	0.211
Pericardial effusion, n (%)	55 (33.5)	31 (52.5)	**0.010**

Left ventricular longitudinal peak systolic strain, % (IQR)		-11.69 (-15.40- -8.70)	-13.20 (-15.40- -10.00)	0.223
Apical sparing of longitudinal strain, n (%)		114 (69.9)	49 (71.0)	0.612
Heart rate, bpm (IQR)		73 (64-81)	84 (69-91)	**<0.001**
Rhythm	Sinus rhythm, n (%)	98 (60.1)	41 (71.0)	0.431
	Atrial fibrillation, n (%)	47 (28.8)	11 (19.4)	
	Atrial flutter, n (%)	5 (3.3)	1 (1.6)	
	Pacemaker, n (%)	13 (7.8)	5 (8.1%)	
Low voltage*, n (%)		21 (11.1)	8 (12.9)	0.292
AV block, n (%)		46 (28.3)	10 (17.7)	**0.004**
PQ interval, ms (IQR)		196 (160-222)	166 (148-192)	**0.003**
Intraventricular conduction delay	LAFB, n (%)	62 (37.9)	16 (27.4)	**0.005**
	LBBB, n (%)	32 (19.6)	5 (8.1)	
	RBBB, n (%)	42 (25.5)	5 (8.1)	
QRS interval, ms (IQR)		120 (95-156)	96 (86-120)	**<0.001**
QTc interval, ms (IQR)		473 (445-503)	469 (446-506)	0.885

Transthyretin cardiac amyloidosis (ATTR-CA); Cardiac light-chain (AL) amyloidosis; New York Heart Association (NYHA); N-terminal prohormone of brain natriuretic peptide (NT-proBNP); modified Look–Locker inversion recovery sequence derived extracellular volume (MOLLI-ECV).; New York Heart Association (NYHA); intracardiac cardioverter defibrillator (ICD); N-terminal prohormone of brain natriuretic peptide (NT-proBNP); left ventricular ejection fraction (LVEF); atrioventricular (AV) block; left anterior fascicular block (LAFB); left bundle branch block (LBBB); right bundle branch block (RBBB)

* Low voltage was defined by an amplitude <0.5 mV in limb leads or <0.75 mV in precordial leads.

Values are given as median and interquartile range (IQR), or total numbers (n) and percent (%).

Bold indicates $p<0.05$.

Supplementary Figures

Figure S1. Study flow chart

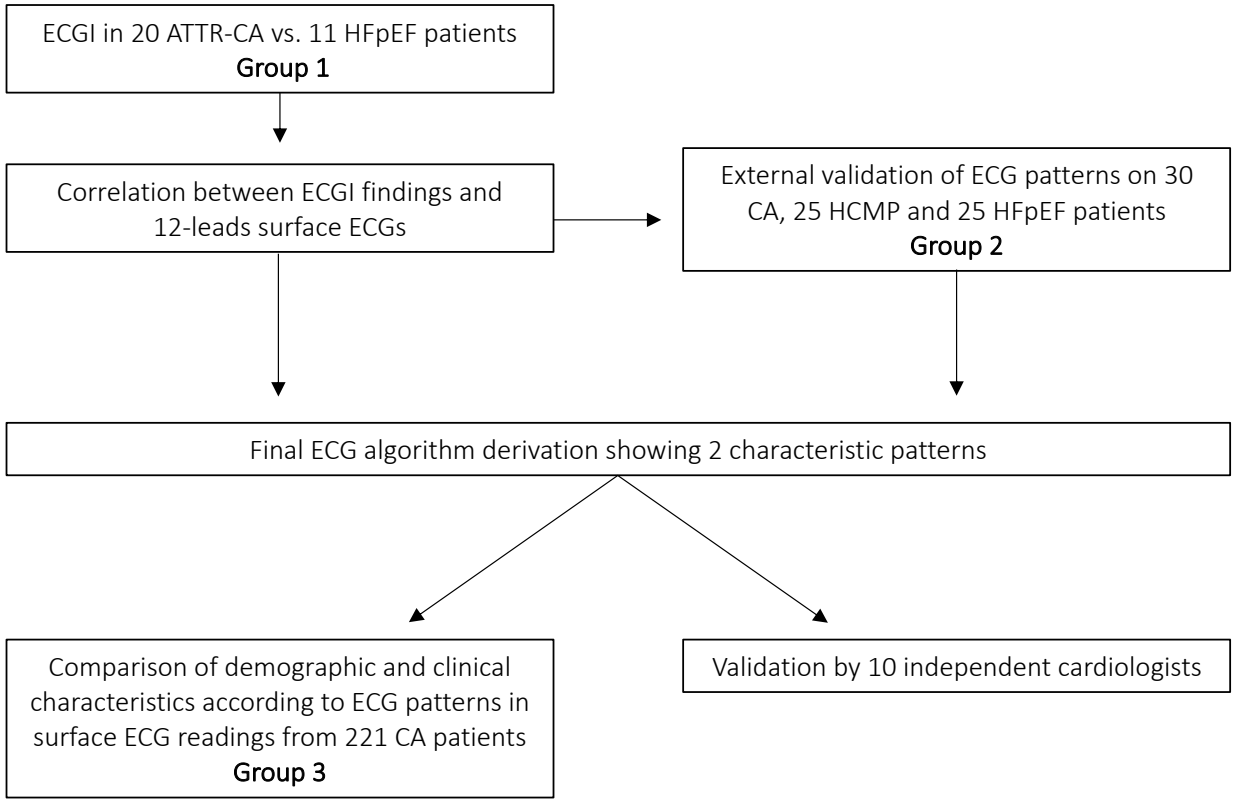

Figure S2. Principal component analysis (PCA) of mean ventricular voltage maps
PCA of the voltage maps from 3 consecutive ventricular beats of CA and controls identifies two distinct clusters (A). Cluster centroid distances of region-specific PCA with respect to voltage patterns in CA and controls show the greatest cluster differences in the basal regions of the left and right ventricles (B).

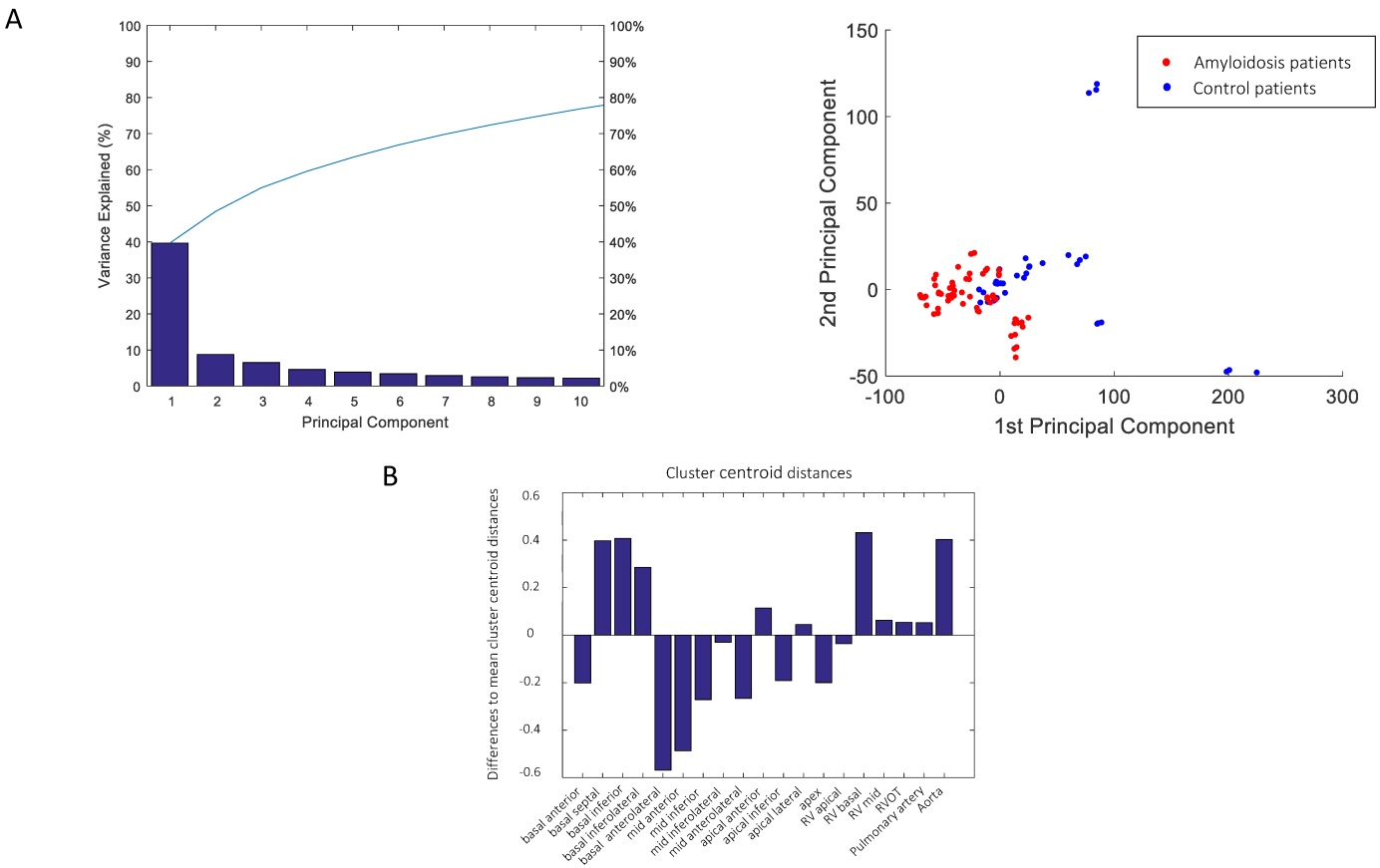

Figure S3. Differences in ECG of CA compared to HCMP and HFpEF
Comparison of mean ECG trace representations of individual ECG traces from 30 CA patients, 25 HCMP patients and 25 HFpEF patients revealed significant differences in respective leads of R-peak timing and R amplitude.

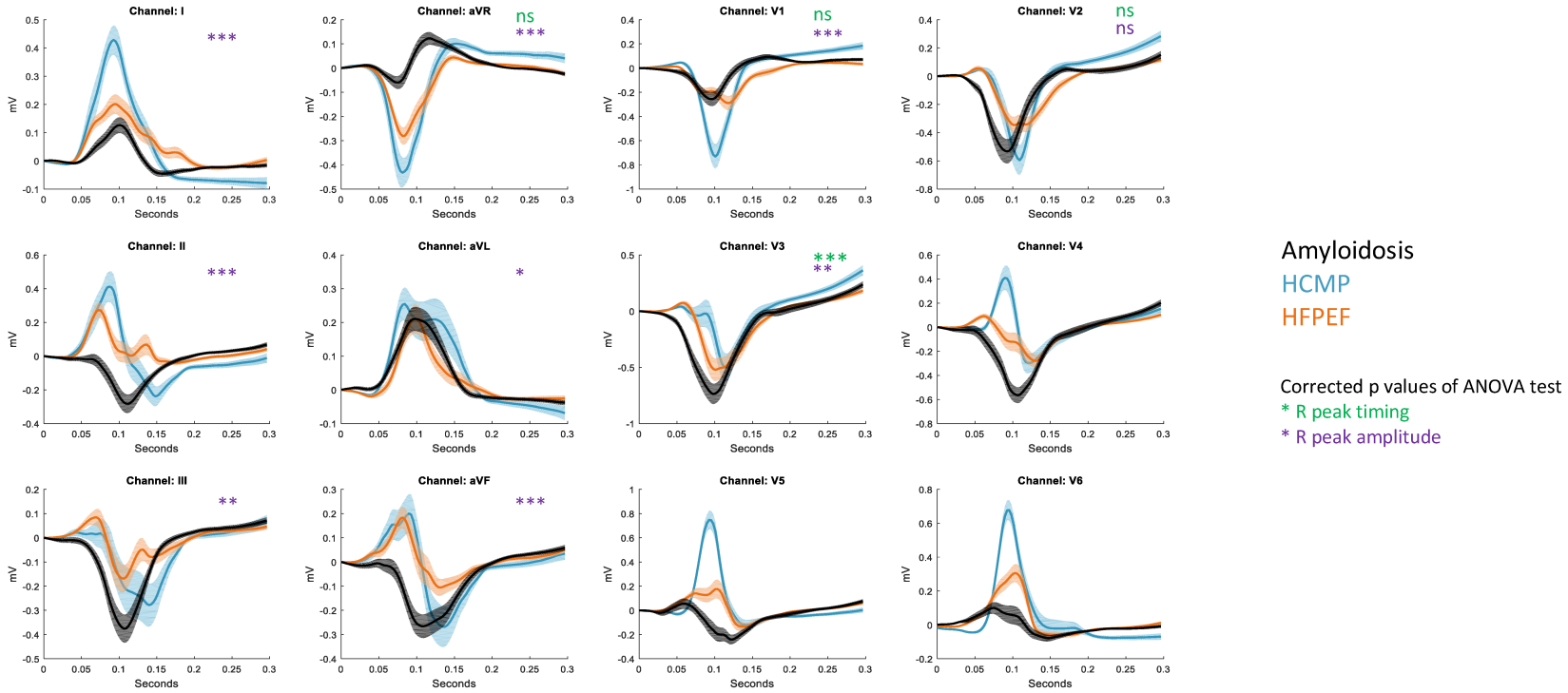

Figure S4. A typical 12-lead ECG example from a patient with cardiac amyloidosis with characteristics of pattern 1, including a delayed R progression in V1 to V3 and an amplitude less than 1 mV in II, III and aVF.

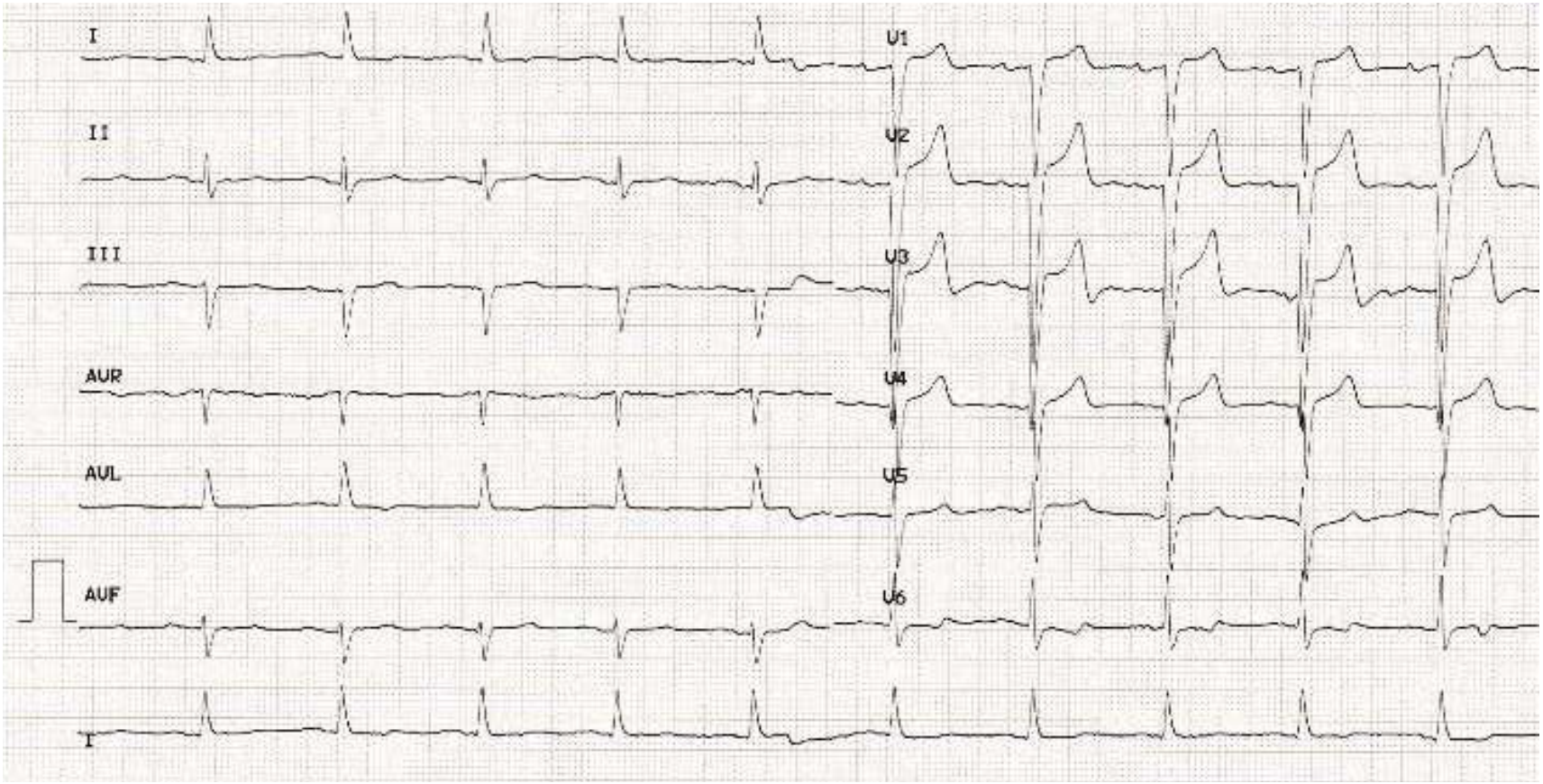

Schrutka L, *et al*. *Heart* 2022; 108:1137–1147. doi: 10.1136/heartjnl-2021-319846

Figure S5. A typical 12-lead ECG example from a patient with cardiac amyloidosis with characteristics of pattern 2, including right bundle branch block and left anterior fascicular block

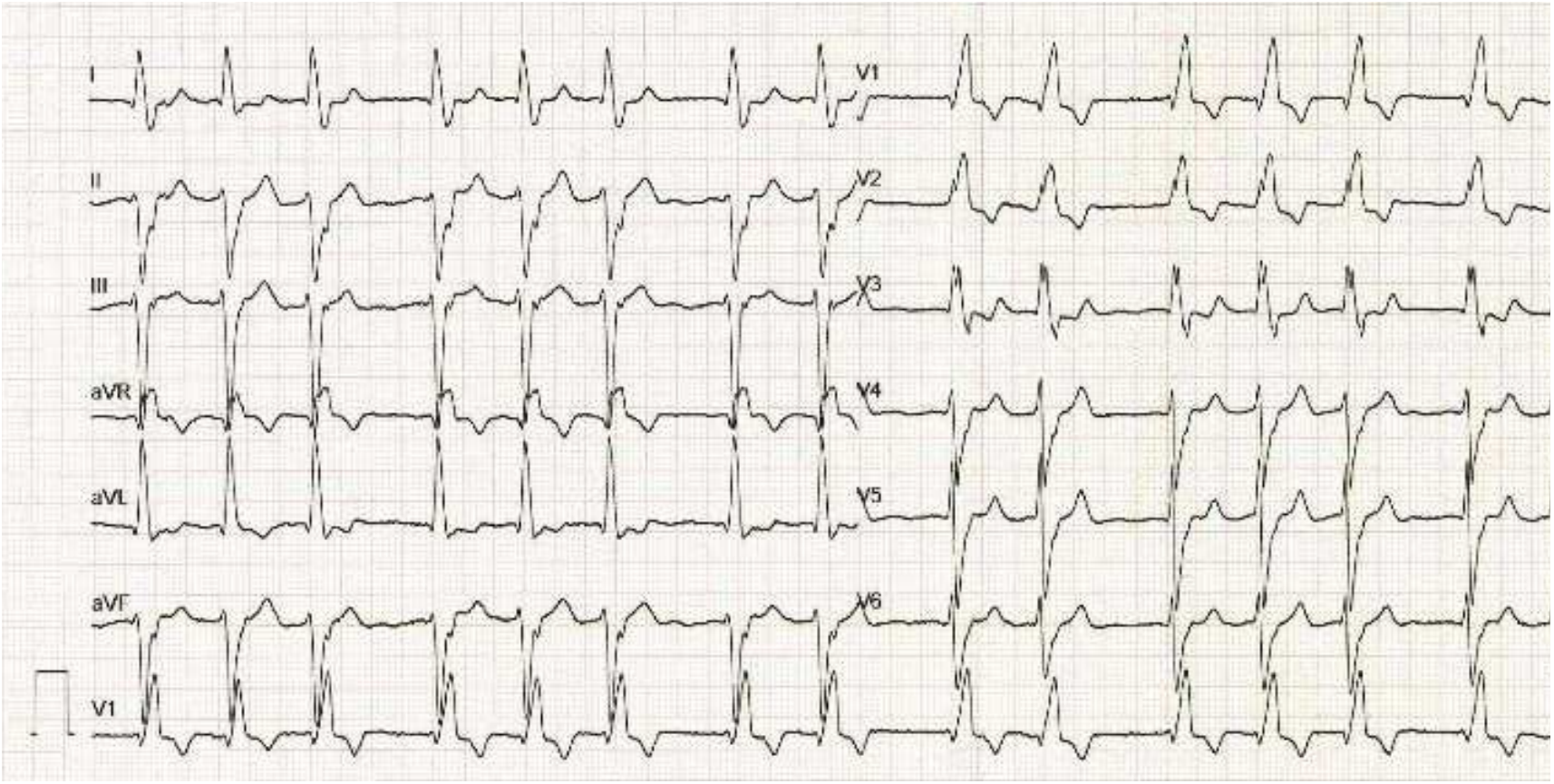

Figure S6. Diagnostic accuracy of the proposed ECG algorithm
Receiver operating curves and corresponding areas under the curve (AUC) of cardiologists interpreting surface ECGs before and after training on the defined ECG patterns demonstrate significant improvements in the detection rate of CA following training.

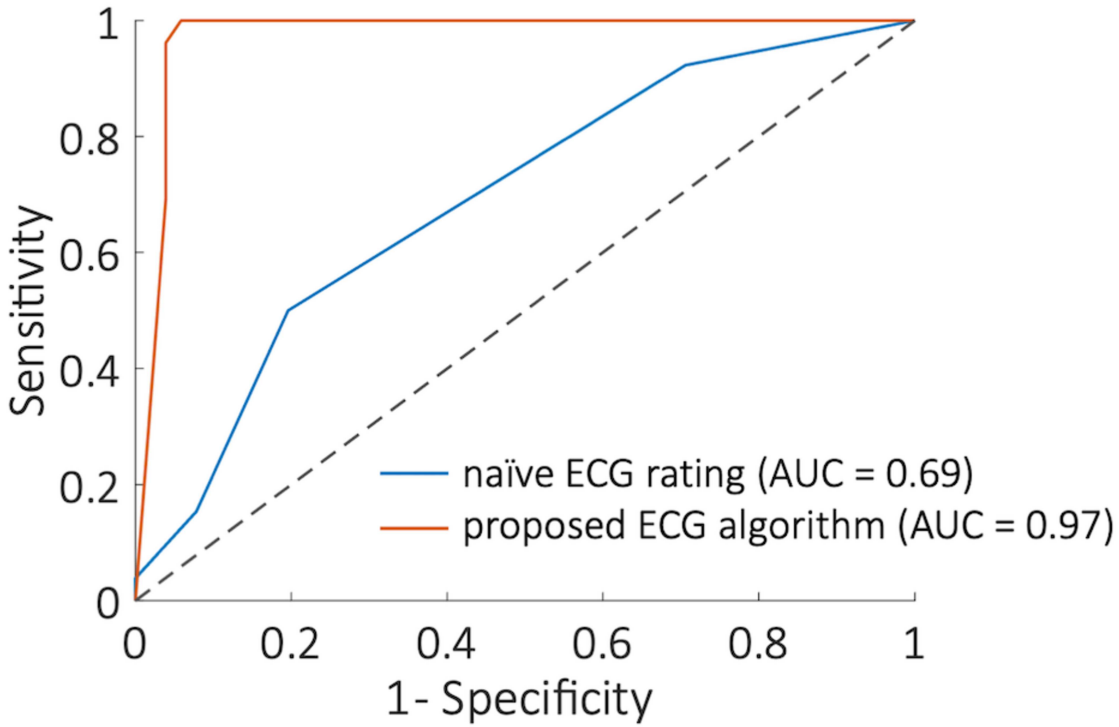

References

1. Gillmore JD, Maurer MS, Falk RH, Merlini G, Damy T, Dispenzieri A, et al. Nonbiopsy Diagnosis of Cardiac Transthyretin Amyloidosis. Circulation. 2016;133(24):2404-12.

2. Gertz MA, Comenzo R, Falk RH, Fermand JP, Hazenberg BP, Hawkins PN, et al. Definition of organ involvement and treatment response in immunoglobulin light chain amyloidosis (AL): a consensus opinion from the 10th International Symposium on Amyloid and Amyloidosis, Tours, France, 18-22 April 2004. Am J Hematol. 2005;79(4):319-28.

3. Dirk-Jan Kroon (2020). Finite Iterative Closest Point (https://www.mathworks.com/matlabcentral/fileexchange/24301-finite-iterative-closest-point) MCFERN, 2020. Finite Iterative Closest Point 2020 [Available from: https://www.mathworks.com/matlabcentral/fileexchange/24301-finite-iterative-closest-point.

4. Audenaert EA, Van Houcke J, Almeida DF, Paelinck L, Peiffer M, Steenackers G, et al. Cascaded statistical shape model based segmentation of the full lower limb in CT. Comput Methods Biomech Biomed Engin. 2019;22(6):644-57.

5. Lang RM, Badano LP, Mor-Avi V, Afilalo J, Armstrong A, Ernande L, et al. Recommendations for cardiac chamber quantification by echocardiography in adults: an update from the American Society of Echocardiography and the European Association of Cardiovascular Imaging. European heart journal cardiovascular Imaging. 2015;16(3):233-70.